Journal of Alloys and Compounds 491 (2010) 668–672

Contents lists available at ScienceDirect

Journal of Alloys and Compounds

journal homepage: www.elsevier.com/locate/jallcom

Preparation and electrochemical characterization of $LiFePO_4$ nanoparticles with high rate capability by a sol–gel method

S.B. Lee [a], I.C. Jang [a], H.H. Lim [a], V. Aravindan [b], H.S. Kim [c], Y.S. Lee [a,*]

[a] Faculty of Applied Chemical Engineering, Chonnam National University, 300 Yongbong-dong, Gwang-ju 500-757, Republic of Korea
[b] The Research Institute for Catalysis, Chonnam National University, 300 Yongbong-dong, Gwang-ju 500-757, Republic of Korea
[c] Korea Electrotechnology Research Institute, 28-1 Seongju-dong, Changwon 641-120, Republic of Korea

ARTICLE INFO

Article history:
Received 22 October 2009
Accepted 3 November 2009
Available online 11 November 2009

Keywords:
$LiFePO_4$
High rate capability
Sol–gel
Adipic acid
Cathode material
Lithium secondary battery

ABSTRACT

The synthesis of $LiFePO_4$ nanoparticles by an adipic acid-assisted sol–gel route has been optimized based on cycling and structural analysis. Formation of the crystalline phase was investigated through thermogravimetric-differential thermal analysis (TG-DTA). Among the optimized conditions, a 0.5 molar ratio of the adipic acid to total metal ions at a 670 °C calcination temperature under an Ar atmosphere yielded $LiFePO_4$ particles with the desired properties. The synthesized particle sizes ranged from 50 to 100 nm. The Li/$LiFePO_4$ cell exhibited an initial discharge capacity of 150 mAh g^{-1} that was maintained for 100 cycles. Elevated temperature (50 °C) performance of the cell is also described, showing a stable discharge behavior up to 60 cycles without any decline in capacity. Furthermore, the cell was subjected to rate capability studies (1–30 C) that suggested excellent capacity retention of the cell at ambient temperature. We conclude that the adipic acid-assisted sol–gel process is an excellent route to product $LiFePO_4$ powders on large scale with high rate capability and retention.

1. Introduction

$LiFePO_4$ is a promising low-cost positive electrode material for lithium-ion batteries slated for powering HEV, electric bicycles, and power tools of various applications. Since the revolutionary work of Padhi et al. [1], this material was found to possess overwhelming advantages given its high theoretical capacity (170 mAh g^{-1}), good cycle life, redox potential (3.5 V) located in the electrochemical stability window of common non-aqueous electrolytes, flat discharge profile, ability to sustain high current rates, low cost, natural abundance, thermal and chemically stability, and environmental soundness over cobalt. With $LiFePO_4$ cathodes in commercial batteries in place of toxic $LiCoO_2$, battery costs could be reduced drastically [2].

The main obstacle in obtaining this goal and theoretical capacity is poor rate capability due to inferior electronic conductivity and low lithium-ion diffusion into $LiFePO_4$–$FePO_4$ interfaces. This inherent conductivity is likely due to its crystal structure. In the olivine structure, there is no continuous network frames of FeO_6 edge-shared octahedra to contribute to electronic conductivity; instead, the divalent Fe^{2+} ions occupy corner-shared octahedra. The lithium ions are located in chains of edge-shared octahedra while the phosphorus ions are positioned in tetrahedral sites [3]. Several approaches have been proposed to circumvent this. In particular, partial substitution of Fe ions by transition metal elements [4], thereby reducing the particle size to nanograins, would lead to a diminution of the diffusion lengths for both electrons and ions. Another approach involves the surface coating of $LiFePO_4$ with a conductive matrix such as carbon [5]. However, $LiFePO_4$ with carbon has proven an excellent alternative in the search of $LiFePO_4$ cathodes [6–8]. Vast numbers of carbon source materials have been used to synthesize $LiFePO_4$ particles *via* solid-state reactions, sol–gel, hydrothermal, microwave, spray pyrolysis, precipitation, and emulsion drying [9–17]. Among them, the sol–gel route is an effective technique to synthesize desired particles sizes with good stoichiometry, low calcination temperatures, and high yields [18]. Herein is reported the synthesis of $LiMn_2O_4$ and $LiNiO_2$ with nanoparticles using adipic acid as a chelating agent to yield excellent battery performance [18,19]. Recently, we successfully synthesized the $LiFePO_4$ nanoparticle by a sol–gel method with excellent cycle characterization under harsh conditions and report the unique powder/electrochemical properties of Li/$LiFePO_4$ cell in this study.

2. Experimental

Nanocrystalline $LiFePO_4$ was synthesized from $LiCH_3COO$, $Fe(CH_3COO)_2$, H_3PO_4, and $C_6H_{10}O_4$, all from Sigma–Aldrich (USA), using a conventional sol–gel method. A stoichiometric amount of each material was dissolved in ethanol and mixed thoroughly with an aqueous solution of the adipic acid chelating agent. First, the starting

* Corresponding author. Fax: +82 62 530 1909.
E-mail address: leeys@chonnam.ac.kr (Y.S. Lee).

0925-8388/$ – see front matter © 2009 Elsevier B.V. All rights reserved.
doi:10.1016/j.jallcom.2009.11.037

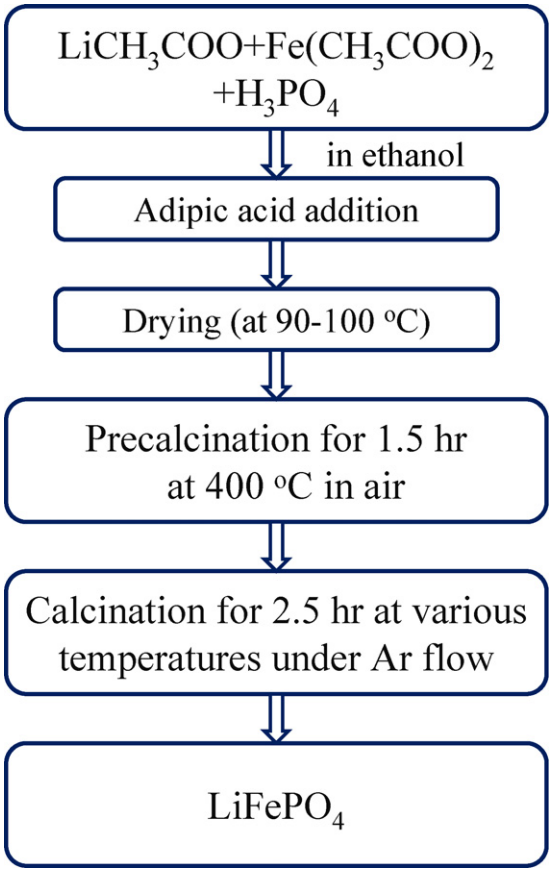

Fig. 1. Pictorial representation of the synthetic process.

materials were dissolved in ethanol and then mixed with different concentrations of adipic acid (hereafter denoted AA) in the form of an aqueous solution. The solution was evaporated at 90 °C for 4 h to form a transparent sol. The sol was then transferred to a vacuum oven and dried at 90–100 °C to yield the gel precursors that were finely ground and calcined at 400 °C for 1.5 h and calcined again at various temperatures ranging from 650 to 700 °C for 2.5 h under argon. The synthesis procedure is graphically illustrated in Fig. 1. Thermal studies were carried out by means of thermogravimetric-differential analysis (TG-DTA) using a thermal analyzer system (STA 1640, Stanton Redcroft Inc., UK). A thin Pt plate was used as the sample holder and the powder heated at 5 °C min^{-1} and cooled at 10 °C min^{-1}. The carbon content of the synthesized $LiFePO_4$ particles was determined using an elemental analyzer (CHN Flash EA series, CE Instruments, Italy). Structural analysis was carried out by powder X-ray diffraction (XRD, Rint 1000, Rigaku, Japan) using CuKα radiation. Particle shape and size distribution of the resulting compound were observed using a transmission electron microscope (TEM, TecnaiF20, Philips, Netherlands) and a particle size analysis system (Mastersizer 2000E, Malvern Instrument, UK), respectively. Cycling performance was studied using a CR2032 coin-type cell. The cathode was fabricated with 20.0 mg of accurately weighed active material, 3.0 mg of Ketzen black, and 3.0 mg of conductive binder (2.0 mg of teflonized acetylene black (TAB) and 1.0 mg of graphite). The material was pressed on a 200 mm^2 stainless steel mesh, used as the current collector under a pressure of 300 kg cm^{-2} and dried at 130 °C for 5 h in an oven. The final cell was composed of a cathode and a metallic lithium anode separated by a porous polypropylene film (Celgard 3401). A mixture of 1.0 M $LiPF_6$–ethylene carbonate (EC)/dimethyl carbonate (DMC) (1:1, v/v, Techno Semichem Co., Ltd., City, Korea) was used as an electrolyte. Cycling studies were carried out at various current rates with a cut-off voltage between 2.8 and 4.0 V (2.5–4.0 V for rate capability testing) at ambient (25 °C) and elevated temperatures (50 °C).

3. Results and discussion

Thermogravimetric-differential thermal analysis (TG-DTA) was used to establish the temperature for precursor preparation. Fig. 2 shows the TG-DTA curves performed on the $LiFePO_4$ precursor, in which the thermal traces clearly shows three main stages. First, stage contains multiple endothermic events that begin near 100 °C

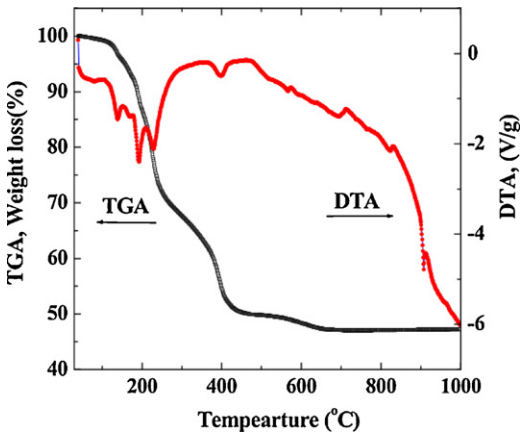

Fig. 2. TG-DTA analysis of starting materials in an Ar atmosphere. The molar ratio of adipic acid to total metal ions was 0.5.

and end at 250 °C; this steep weight loss of ~28% is ascribed to the removal of residual moisture (including water absorbed during sample loading) and decomposition of acetate groups from the starting materials. This weight loss was also inclusive of the melting of AA. The second melting event that began between 251 and 450 °C can be attributed to the decomposition of the reactants with carbonization of AA and crystallization of $LiFePO_4$, with a weight loss of about 21%. Finally, the slow and gradual weight loss above 450–650 °C, with one kink-like appearance of a melting event, corresponds to decomposition of the remaining reactants and carbon oxidation, producing either carbon monoxide or carbon dioxide [20]. From the TG-DTA analysis, the precursor was heat-treated at temperatures above 650 °C for the synthesis of $LiFePO_4$ with AA as the chelating agent.

Fig. 3 displays the XRD patterns of the $LiFePO_4$ powders treated at different calcination temperatures. Optimization of temperature was necessary to obtain material with good crystallinity and without impurities. The lower temperature XRD pattern (650 °C), as well as higher temperature (700 °C), presents many impurity peaks (marked with * in Fig. 3), such as iron(II, III) pyrophosphates or phosphates ($Li_3Fe_2(PO_4)_3$ or Li_3PO_4) [21]. However, these impurity peaks disappear and other main peaks sharpen upon increasing temperature, indicating that increase in crystallinity may be a result of growth of grain size, well ordered structure, and release of lattice strain. The variation of calcination temperature on the lattice

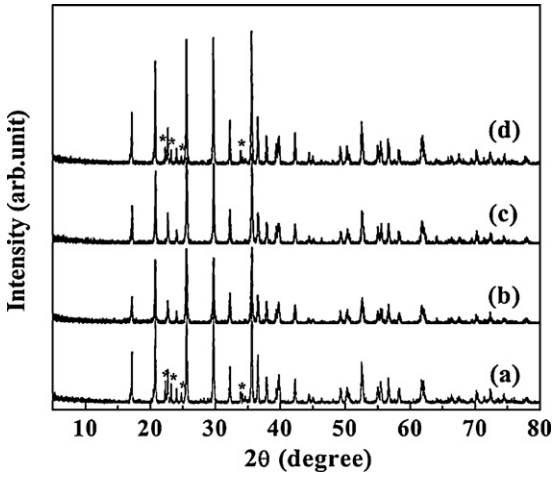

Fig. 3. XRD patterns with various calcination temperatures for 2.5 h under argon: (a) 650 °C, (b) 660 °C, (c) 670 °C, and (d) 700 °C (*impurity phases, likely $Li_3Fe_2(PO_4)_3$ or Li_3PO_4).

Table 1
Powder properties of $LiFePO_4$ materials obtained at different calcinations temperatures.

Temperature (°C)	a (Å)	b (Å)	c (Å)	α (°)	β (°)	γ (°)	V (nm^3)
650	10.307	6.009	4.693	90	90	90	0.2906
660	10.307	5.993	4.689	90	90	90	0.2897
670	10.322	6.005	4.691	90	90	90	0.2909
700	10.327	6.008	4.693	90	90	90	0.2912

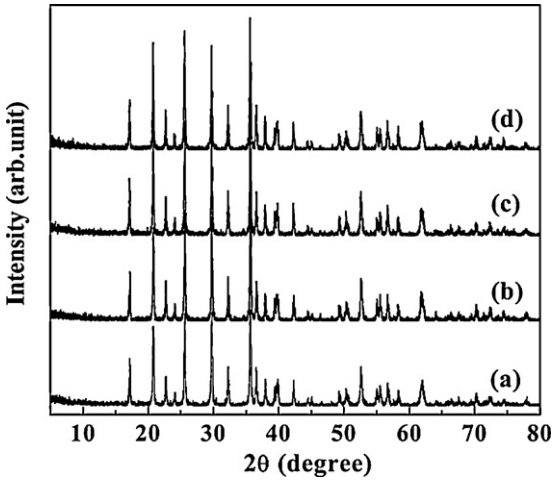

Fig. 4. XRD patterns of different molar ratios of adipic acid to total metal ions: (a) 0.2, (b) 0.5, (c) 1.0, and (d) 1.5.

constants of the $LiFePO_4$ materials is shown in Table 1. The lattice constants of the $LiFePO_4$ material obtained at 670 °C, without impurities, are similar to those previously reported (a = 10.3308 Å, b = 6.0081 Å, c = 4.6994 Å) [22]. In addition, this lab confirmed that the capacity of the $LiFePO_4$ decreased as the temperature rose above or dropped below 670 °C in the electrochemical cell test (capacity profiles not given in this manuscript). A possible explanation for this is that high temperature induces the agglomeration and growth of such particles while reducing the reactivity of carbon and as such, leads to formation of impurity phases at high temperatures, like Fe_2P [23]. Nevertheless, lower temperatures can cause a premature termination of the crystallization process and increase the possibility of forming trivalent iron impurities due to oxidation of Fe^{2+} ions [24].

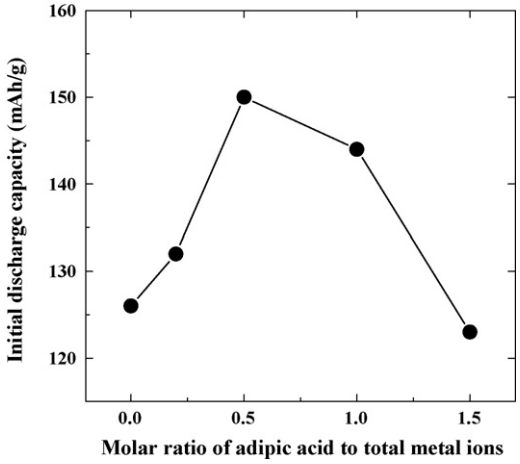

Fig. 5. Initial discharge capacity of the Li/$LiFePO_4$ cell obtained by various molar ratios of adipic acid to total metal ions.

Fig. 4 shows the X-ray diffraction patterns of various molar ratios of adipic acid to total metal ions calcined at 670 °C for 2.5 h under an Ar atmosphere. The entire diffraction peaks can be attributed to a well ordered olivine crystalline phase. It is difficult to detect impurities like Fe_2S and $Fe_3(PO_4)_2$ phases in all samples by XRD measurements. Thus, optimization of AA should be made only through cycling performance of the material.

Fig. 5 presents the cycling performances of different concentrations of AA were performed at ambient temperature. At lower molar ratios (0.2), the cell delivered a discharge capacity of only 132 mAh g^{-1}. When increasing the AA molar ratio from 0.2 to 0.5, the discharge capacity was remarkably improved and the difference between the two materials was approximately 18 mAh g^{-1}. The molar ratio of the AA exceeded 0.5 as the discharge capacity tended to decrease. A decrease in discharge capacity beyond 0.5 may result in a higher residual carbon content from starting materials and lead to the formation of more inactive phases on the surface. This residual carbon also suppresses crystallization behavior while excess carbon can dilute the active particle distance, leading to capacity fading and columbic efficiency. Further, at temperatures beyond 670 °C, the residual carbon may reduce Fe and P to form an inactive Fe_2P phase on the surface [23,25].

Fig. 6 shows the particle size distribution and particle morphological features of the $LiFePO_4$ by TEM images. The molar ratio of

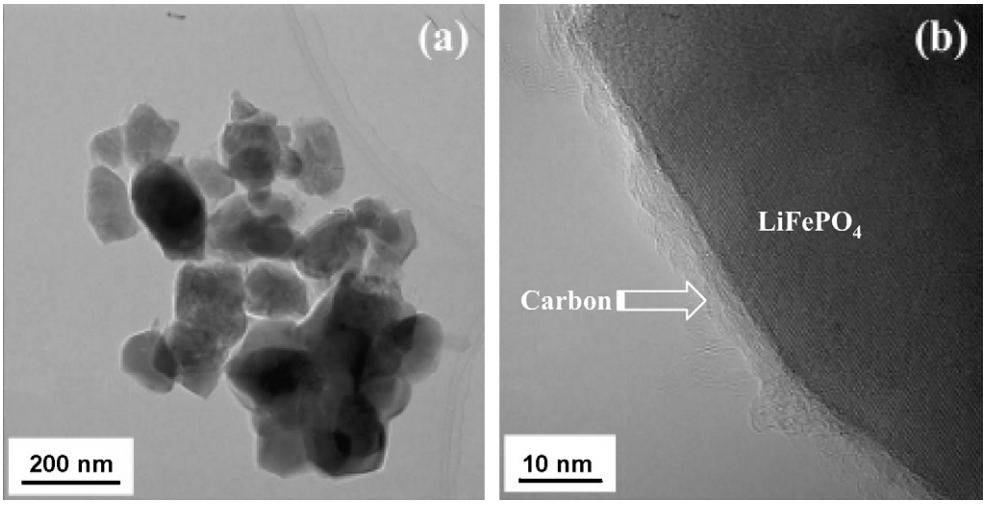

Fig. 6. (a) TEM image and (b) carbon coating layer on $LiFePO_4$ obtained by the sol–gel route.

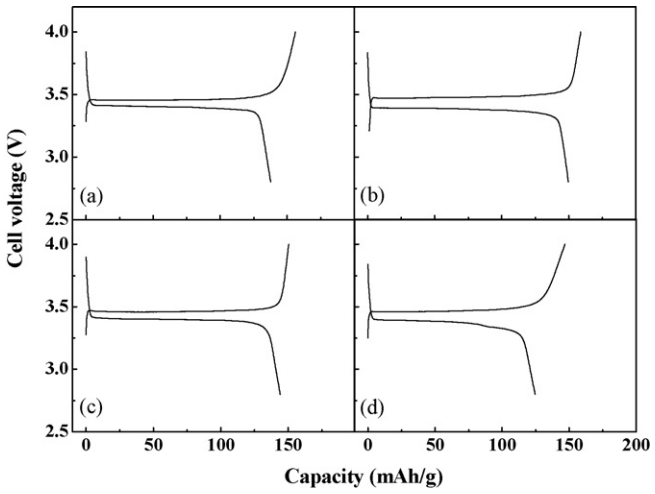

Fig. 7. The first cycle behavior of Li/$LiFePO_4$ cells at room temperature obtained at various molar ratios of adipic acid to total metal ions: (a) 0.2, (b) 0.5, (c) 1.0, and (d) 1.5.

adipic acid to total metal ions was 0.5. The TEM image clearly indicates that $LiFePO_4$ is mainly composed of very small polycrystalline materials ranging from 50 to 100 nm. The high surface area of such evenly distributed nanocrystalline materials improves the electrochemical performance of the cell by shortening the diffusion length of the lithium ions. Interestingly, the particles of $LiFePO_4$ obtained by the sol–gel method were coated with carbon, which resulted from use of the adipic acid as a chelate agent during synthesis. The carbon content of the $LiFePO_4$ particle was analyzed by carbon analysis with a content of about 2.84 wt.% when the molar ratio of the AA was 0.5. It was expected that direct carbon coating on the $LiFePO_4$ by residual carbon, during synthesis, may contribute to enhancement of electronic conductivity, as well as improve the sluggish kinetics behavior.

Fig. 7 shows the initial charge/discharge curves of the Li/$LiFePO_4$ cell at various molar ratios of adipic acid to total metal ions (0.2–1.5) calcined at 670 °C for 2.5 h under an Ar atmosphere. All Li/$LiFePO_4$ cells exhibited the typical electrochemical behavior with a long distinct plateau near ~3.4 V in the first charge/discharge process at ambient temperature. A high initial charge capacity of ~159 mAh g^{-1} for the cell when a 0.5 molar ratio of AA was observed, however, presented a slightly reduced discharge capacity (150 mAh g^{-1}). This may be due to formation of a solid electrolyte interface (SEI) on the surface of the electrodes. After exceeding a 0.5 molar ratio, the Li/$LiFePO_4$ cells abruptly decreased in initial discharge capacity with an unstable discharge curve in the 3.25 V region when the molar ratios were 1.5. From these results, it can expected that the charge/discharge behavior of the $LiFePO_4$ material is strongly related to the content of the adipic acid, a carbon coating source on the $LiFePO_4$ powder, and can determine the best optimized conditions of synthesis of this material.

Fig. 8 presents the cycle performance of the optimized Li/$LiFePO_4$ cell calcined at 670 °C for 5 h under Ar atmosphere with an adipic acid to total metal ions molar ratio of 0.5. Two cells were cycled at 0.1 mA cm^{-2} between 2.8 and 4.0 V, at room (25 °C) and high (50 °C) temperatures. For the Li/$LiFePO_4$ cell at room temperature, no capacity fade was observed from the third cycle onwards up to 100 cycles (>99.9%) as the cell experienced a stable discharge behavior (153 mAh g^{-1}), appearing as a straight line. This remarkable cycling behavior may be attributed to the synthesis of the $LiFePO_4$ *via* the AA-assisted sol–gel route [26]. Elevated temperature (50 °C) cycling performances of the cell also present similar behavior compared to room temperature test. Surprisingly, the cell exhibits stable and similar discharge behavior to that of room temperature conditions with the same capacity of up to 50 cycles. After that, the SEI was broken, leading to drastic capacity fade, and finally short-circuiting of the electrodes. Although there may be various reasons for the cell failure, it is the contention of the authors that it is due to the dissolution of Fe^{2+} ions in the electrolyte [27–30] as a trace amount of water (<1 ppm) in the electrolyte solution can lead to the formation of dangerous HF. At high operational temperatures, HF can break the SEI and dissolve Fe^{2+} ions in the electrodes [30]. Experimentation within this lab is underway to test and reveal the cycle mechanism of the Li/$LiFePO_4$ cells at high temperatures.

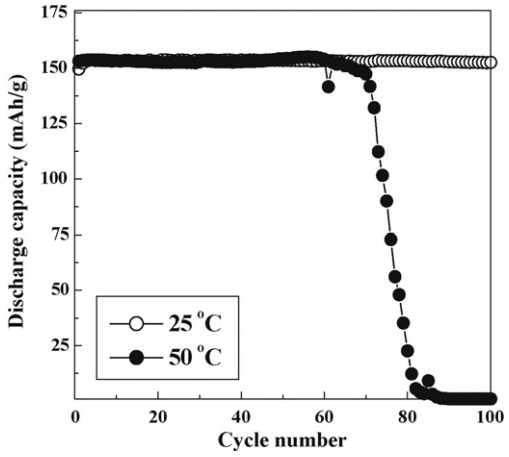

Fig. 8. Discharge capacity profile with number of cycles of the Li/$LiFePO_4$ cell at (a) room (25 °C) and (b) elevated temperatures (50 °C).

Recently, several authors reported the high rate capabilities of Li/$LiFePO_4$ cells derived from the sol–gel approach with high discharge capacity and good cycle retention [15,31–34]. In particular, Choi and Kumta [34] reported a lauric acid-assisted sol–gel route to obtain $LiFePO_4$ nanoparticles. This material exhibits superior performance at a 10 C rate with a discharge capacity greater than 125 mAh g^{-1}. However, the authors presented the cycling performance of the cell for only 33 cycles and up to a 10 C rate only. In this study, the rate capability of the Li/$LiFePO_4$ cell was studied with different current densities from 1 to 30 C and between 2.5 and 4.0 V, an enlarged cut-off voltage to create more harsh conditions at room temperature. For example, as shown in Fig. 9, at a 1 C rate, the cell showed a high capacity of 148 mAh g^{-1} that was reduced to 59 mAh g^{-1} at a high current rate of 30 C. Then, the cur-

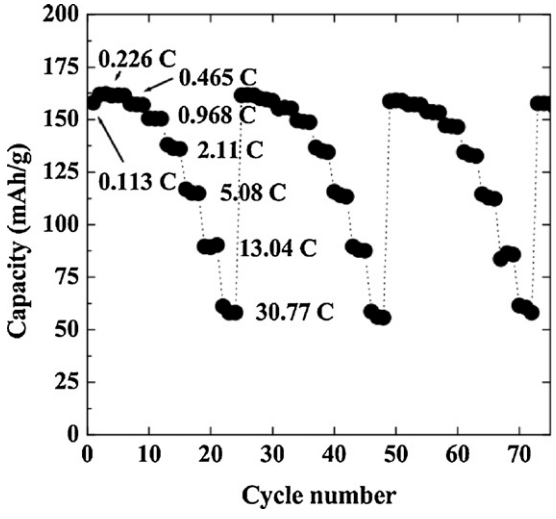

Fig. 9. Rate capability performance of the Li/$LiFePO_4$ cell at room temperature.

rent rate is again changed to 1 C in an iterative fashion; all the while, the cell maintains the former capacity. This excellent rate capability performance of the Li/$LiFePO_4$ cell under harsh conditions may be ascribed to the optimum particle size from 150 to 100 nm and carbon coating, a direct result of the sol–gel synthetic process employing adipic acid as a chelating agent [26].

4. Conclusions

In conclusion, the adipic acid concentration and calcination temperature were optimized based on cycling and structural studies. Nanocrystalline $LiFePO_4$ particles were synthesized by a sol–gel process at 670 °C in an Ar atmosphere at an optimized 0.5 molar ratio of adipic acid to total metal ions. The obtained $LiFePO_4$ composed the vast majority of the particles between 50 and 100 nm. The Li/$LiFePO_4$ cell experienced an initial discharge capacity >150 mAh g^{-1} at ambient and elevated temperatures (50 °C). No capacity fade was observed at ambient temperature up to 100 cycles, whereas the cell was degraded due to dissolution of Fe^{2+} ions at elevated temperatures beyond 60 cycles. Furthermore, the Li/$LiFePO_4$ cell was employed at various current rates, from 1 to 30 °C as a cycle, and resulted in excellent capacity retention of the cell. The adipic acid-assisted sol–gel process is an excellent route to production of $LiFePO_4$ particles on large scale with high rate capability and retention.

Acknowledgements

This work was supported by a grant (Code#: 2009K000446) from the 'Center for Nanostructured Materials Technology', under the '21st Century Frontier R&D programs' of the Ministry of Education, Science and Technology, Korea.

References

[1] A.K. Padhi, K.S. Nanjundswamy, J.B. Goodenough, J. Electrochem. Soc. 144 (1997) 1188–1194.
[2] A. Ritchie, W. Howard, J. Power Sources 162 (2006) 809–812.
[3] M. Thackeray, Nat. Mater. 1 (2002) 81–82.
[4] S.Y. Chung, J.T. Bloking, Y.M. Chiang, Nat. Mater. 1 (2002) 123–128.
[5] A.K. Shukla, T.P. Kumar, Curr. Sci. India 94 (2008) 314–331.
[6] A. Singhal, G. Skandan, G. Amatucci, F. Badway, N. Ye, A. Manthiram, H. Ye, J.J. Xu, J. Power Sources 129 (2004) 38–44.
[7] F.K. Hsu, S.Y. Tsay, B.J. Hwang, J. Mater. Chem. 14 (2004) 2690–2695.
[8] M. Takahashi, H. Ohtsuka, K. Akuto, Y. Sakurai, J. Electrochem. Soc. 152 (2005) A899–A904.
[9] R. Dominko, M. Bele, M. Gaberscek, M. Remskar, D. Hanzel, J.M. Goupil, S. Pejovnik, J. Jamnik, J. Power Sources 153 (2006) 274–280.
[10] S. Yang, P.Y. Zavaliji, M.S. Whittingham, Electrochem. Commun. 3 (2001) 505–508.
[11] J. Barker, M.Y. Saidi, J.L. Swoyer, Electrochem. Solid-State Lett. 6 (2003) A53–A55.
[12] C. Delacourt, P. Poizot, S. Levasseur, C. Masquelier, Electrochem. Solid-State Lett. 9 (2006) A352–A355.
[13] V. Palomares, A. Goni, I.G.D. Muro, I.D. Meatza, M. Bengoechea, O. Miguel, T. Rojo, J. Power Sources 171 (2007) 879–885.
[14] C. Delmas, M. Maccario, L. Crogunnec, F.L. Cras, F. Weill, Nat. Mater. 7 (2008) 665–671.
[15] A. Manthiram, A.V. Murugan, A. Sarkar, T. Muraliganth, Energy Environ. Sci. 1 (2008) 621–638.
[16] D. Jugovic, D. Uskokovic, J. Power Sources 190 (2009) 538–544.
[17] Z. Li, D. Zhang, F. Yang, J. Mater. Sci. 44 (2009) 2435–2443.
[18] Y.S. Lee, Y.K. Sun, K.S. Nahm, Solid State Ionics 109 (1998) 285–294.
[19] Y.S. Lee, Y.K. Sun, K.S. Nahm, Solid State Ionics 118 (1999) 159–168.
[20] L.N. Wang, X.C. Zhan, Z.G. Zhang, K.L. Zhang, J. Alloy. Compd. 456 (2008) 461–465.
[21] F. Gao, Z. Tang, J. Xue, Electrochim. Acta 53 (2007) 1939–1944.
[22] S.T. Myung, S. Komaba, N. Hirosaki, H. Yashiro, N. Kumagai, Electrochim. Acta 49 (2004) 4213–4222.
[23] S.S. Zhang, A.L. Allen, K. Xu, T.R. Jow, J. Power Sources 147 (2005) 234–240.
[24] A. Yamada, S.C. Chung, K. Hinokuma, J. Electrochem. Soc. 148 (2001) A224–A229.
[25] G.T.K. Fey, T.L. Lu, F.Y. Wu, W.H. Li, J. Solid State Electrochem. 12 (2008) 825–833.
[26] S.B. Lee, S.H. Cho, S.J. Cho, G.J. Park, S.H. Park, Y.S. Lee, Electrochem. Commun. 10 (2008) 1219–1221.
[27] R. Oesten, U. Heider, M. Schmidt, Solid State Ionics 148 (2002) 391–397.
[28] K. Amine, J. Liu, I. Belharouak, Electrochem. Commun. 7 (2005) 669–673.
[29] M. Koltypin, D. Aurbach, L. Nazar, B. Ellis, Electrochem. Solid-State Lett. 10 (2007) A40–A44.
[30] M. Koltypin, D. Aurbach, L. Nazar, B. Ellis, J. Power Sources 174 (2007) 1241–1250.
[31] G.X. Wang, S. Bewlay, J. Yao, J.H. Ahn, S.X. Dou, H.K. Liu, Electrochem. Solid-State Lett. 7 (2004) A503–A506.
[32] J. Yang, J.J. Xu, Electrochem. Solid-State Lett. 7 (2004) A515–A518.
[33] C.R. Sides, F. Croce, V.Y. Young, C.R. Martin, B. Scrosati, Electrochem. Solid-State Lett. 8 (2005) A484–A487.
[34] D. Choi, P.N. Kumta, J. Power Sources 163 (2007) 1064–1069.